Reaction Rates in Ultrasonic Emulsions of Dense Carbon Dioxide and Water

Michael T. Timko and Kenneth A. Smith
Dept. of Chemical Engineering, Massachusetts Inst. of Technology, Cambridge, MA 02139

Rick L. Danheiser and Jeffrey I. Steinfeld
Dept. of Chemistry, Massachusetts Inst. of Technology, Cambridge, MA 02139

Jefferson W. Tester
Dept. of Chemical Engineering and Laboratory for Energy and the Environment, Massachusetts Inst. of Technology, Cambridge, MA 02139

DOI 10.1002/aic.10688
Published online November 4, 2005 in Wiley InterScience (www.interscience.wiley.com).

Power ultrasound provides a surfactant-free means of emulsifying dense near-critical carbon dioxide and water. Droplet size distributions and volume fractions of the dispersed phases have been measured for acoustically formed emulsions. Hydrolysis rates were measured for a series of 7 benzoyl halides under both silent, phase-separated conditions and for sonicated, emulsified conditions (30°C, 80 bar, 0.6 W/cm^3, 20 kHz). Sonication always accelerated the overall hydrolysis rate, sometimes by as much as 200-fold. Two physical models were developed to describe global kinetics: one for silent and one for sonicated conditions. The model for silent conditions agreed well with the available data set and suggested conditions under which reaction in the carbon dioxide phase (rather than the water phase) might become important. The model for sonicated conditions properly captured the trends in the data set and predicted the experimental results to within a factor of 2 in the worst case. Our analysis strongly suggests that ultrasound accelerates phase-transfer reactions by increasing the water/carbon dioxide interfacial area. *AIChE J,* 52: 1127–1141, 2006
Keywords: ultrasound, supercritical, water, carbon dioxide, emulsion

Introduction

Many conventional organic solvents are harmful to the environment, and their replacement with benign alternatives is an important step toward achieving the goal of green chemical processing.[1,2] Because they are non-toxic, non-flammable, and readily available, water and carbon dioxide are attractive alternative solvents. Over the past decade, great efforts have been made to increase the utilization of both solvents as reaction media. Several reviews detail the development of synthetic chemistry in aqueous environments[3,4] and in near-critical, dense liquid, or supercritical carbon dioxide ($scCO_2$, T_C = 31.1°C, P_C = 73.8 bar).[5-7]

A key limitation of $scCO_2$ and water is the low solubility of many compounds in either solvent. While ionic and polar compounds dissolve readily in room temperature water, the water solubility of most nonpolar organic compounds is poor. Near-critical and $scCO_2$, on the other hand, are good solvents for some nonpolar organic compounds, including many fluorocarbons.[8-10] Ionic and high molecular weight polar compounds (>100 Da) are essentially insoluble in carbon dioxide under moderate conditions.[11]

Correspondence concerning this article should be addressed to K. A. Smith at kas@mit.edu.

The solvation powers of dense $scCO_2$ and water are complementary, suggesting their combination as a hybrid solvent system. At conditions near the critical point of carbon dioxide, the two fluids are sparingly miscible[12-15] and their mixtures are naturally phase-separated. The resulting interfacial mass transport resistances can be a severe limitation for commercial processes. A recent study of cyclohexene epoxidation in a phase-separated water/carbon dioxide environment[16] is particularly relevant. Based on kinetic measurements, the epoxidation reaction was judged to be impractical in the biphasic system because of the low water solubility of the olefin and its slow rate of mass transport to the aqueous phase.

Dispersion of $scCO_2$ and water as emulsions or microemulsions is an attractive means to increase mass transport. The development of CO_2-philic polymers and surfactants[8,9,17-19] has driven research on both the fundamental aspects and engineering applications of emulsions[20-24] containing the two green solvents. These dispersions have already been used to facilitate a variety of chemical reactions involving small molecules.[25-34] In the carbon dioxide/water system, Jacobsen et al.[25] reported a 10-fold increase in the hydrogenation rate of styrene in an emulsion relative to that measured under phase-separated conditions. An additional benefit of these biphasic solvent systems is that they naturally segregate reactants, products, and catalysts into different phases, and thus may reduce the cost of post-reaction separations.[31,33]

Addition of surfactants to mixtures of carbon dioxide and water has both economic and environmental drawbacks, and a surfactant-free dispersal technique is of great practical interest. Without surfactants, extremely high local energy densities are required to form the micron-sized droplets most desirable for reducing mass transport resistances. Power ultrasound is an efficient means of generating high energy densities, and this makes it an attractive technique for emulsifying mixtures of $scCO_2$ and water.

In this article, we build on a previous experimental study of ultrasonic emulsification[34] for increasing the interfacial contact area between carbon dioxide and water. Here, we develop a quantitative understanding of interfacial mass transport in acoustically agitated systems, an analysis which has heretofore not been available.[35] Mathematical models, combined with new kinetic data and more thorough characterization of the emulsions, confirm that ultrasound accelerates the overall kinetics of phase-transfer reactions by increasing the interfacial contact area, though more subtle effects related to the dynamic nature of our emulsions are also important. Understanding the effects of reactant hydrophobicity, reactivity, and mass transport on global reaction dynamics in biphasic water/carbon dioxide mixtures will assist reactor design and provide an impetus for the development of new reaction systems that exploit the properties of this unique solvent system.

Experimental Procedures

Detailed descriptions of experimental equipment and procedures may be found in Timko.[36]

Materials

Grade 5.5 carbon dioxide (certified purity greater than 99.999%) was purchased from BOC Gases and used as received. Water was deionized (Barnstead, Nanopure) to a minimum resistivity of 18.0 $M\Omega \cdot cm$ and used immediately. Solvents (e.g., acetonitrile, tetrahydrofuran, and benzaldehyde) were purchased from Sigma–Aldrich at greater than 99.5% purity and used as received. Benzoyl halides were purchased from Sigma–Aldrich at purities of 98% or greater and used within 2 weeks of their delivery to minimize hydrolysis during storage.

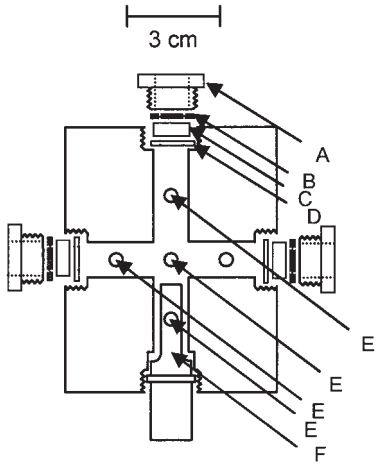

Figure 1. Custom-built high-pressure reactor used for sonication experiments.

A: Stainless steel gland; B: buna–*N* gasket; C: sapphire window; D: Teflon gasket; E: 1/4" apertures for machined NPT fittings; F: sonic probe.

Apparatus

A high-pressure reactor, consisting of two intersecting cylindrical chambers (i.d. = 1.9 cm) bored in a slab (18.8 cm × 15.3 cm × 5.1 cm) of 316-stainless steel, was designed and built for this study. Figure 1 provides a schematic of the reactor. Three of the four apertures in the reactor contained α–Al_2O_3 (sapphire) windows sealed with stainless steel glands. The pressure seal was achieved by using a Teflon gasket. The sapphire itself was protected from damage during tightening by a buna–*N* rubber gasket (90 durometer on the Shore A scale, New England Die Cutting, Inc.). The fourth aperture contained a titanium sonic probe (o.d. = 0.80 cm, Sonics and Materials, Inc.) sealed with a stainless steel gland. The sonic probe is described in greater detail in the next section. The pressure seal on the sonic probe was a combination of a Teflon and a buna–*N* gasket similar to that used for the seals on the windows. The internal volume of the reactor was measured as $87.2 \pm 0.4\ cm^3$.

Five 1/4 in. threaded openings (NPT) were bored into the reactor. The reactor was equipped with a piezoelectric pressure transducer (Dynisco, 832)/digital pressure indicator (Dynisco, 1290) with an accuracy specified as ±1 bar. Operating the reactor for 18-24 hr resulted in less than a 5% drop in system pressure; a typical pressure drop was 2 bar from an initial pressure of 80 bar. The fluid temperature within the reactor was measured using an immersed T-type thermocouple (Omega) with a listed accuracy of ±0.5°C. Reactor temperature was maintained to within ±1.0°C by a combination of a PID controller (Omega, 9001CN) and thermal tape (rated at 100 W output and purchased from Barnstead). In preliminary experi-

ments, the location of the thermocouple probe was varied systematically to ensure that the reactor was reasonably isothermal (to within roughly ± 1.0°C) during sonication.

A dual piston reciprocating pump (Milton Roy/LDC Analytical minipump p/n 92014903), with a maximum flow rate of 25 cm^3/min, was used to recirculate the contents of the vessel and to provide agitation. Independent agitation of the reactor contents was effected by use of a Teflon-coated magnetically coupled stir bar.

The equipment peripheral to the reactor is standard, and only the essential elements are described: (1) a cylinder of liquid carbon dioxide equipped with a dip tube; (2) a heat exchanger system supplied with cold water from a refrigerated circulator (Cole–Parmer, Polystat model), used to liquefy gaseous carbon dioxide prior to further pressurization; (3) a high pressure pump (Eldex, BBB–4) to deliver carbon dioxide to the vessel; and (4) a piezoelectric pressure gauge (Dynisco, 833)/pressure indicator (Dynisco, μPR 690) assembly to measure system pressure. As a safety precaution, the system was also equipped with pressure relief valves rated at 300 bar, which were positioned directly after the pump. The peripheral equipment was isolated from the ultrasonic reactor by an Autoclave Engineering needle valve and a Whitey ball valve in series.

Ultrasound technique

Power ultrasound was introduced directly to the contents of the reactor by a custom-built (Sonics and Materials, Inc.) titanium alloy (90% Ti; 6% Al; 4% V) horn. Mechanical vibration was induced in this horn by a standard piezoelectric converter and ultrasonic processor obtained from Branson (Sonifier 400). The amplitude setting was calibrated against power input to the reactor by using a standard calorimetric technique.[37] We report the average power input to the system during a pulse of sonic irradiation, divided by the known volume of the reactor.

Volume fraction measurements

Sonication of mixtures of dense carbon dioxide and water (approximately 50:50, v/v) results in simultaneous formation of both carbon dioxide/water and water/carbon dioxide emulsions (see Timko[34] for photographs). As a result, the phase ratios present in the emulsions were unknown *a priori*. A chemical tracer technique was used to measure these volume fractions. Octane (for measurement of the carbon dioxide volume fraction in the carbon dioxide/water emulsion) and potassium nitrate (for measurement of the water fraction in the water/carbon dioxide emulsion) were selected as tracers for the two phases. These tracer compounds were useful because they partition quantitatively into the dispersed phases, are chemically inert and nearly surface inactive, and are readily quantified in dilute solutions.

During a typical run, known quantities of the tracer and water were added directly to the reactor. After pressurization with carbon dioxide to 80 bar and heating to 30°C, the contents were emulsified by power ultrasound (20 kHz, 25% duty for a 1 s cycle). Preliminary experiments suggested that emulsions were formed after 10 s of pulsed sonic irradiation; 2 min of sonication ensured that steady state had been reached. Emulsions were sampled through a short section of 316-stainless steel tubing (2.5 mm i.d.) inserted directly into the reactor. The probe was positioned in the reactor in such a way that the desired emulsion phase would be sampled, and visual observation through the sapphire windows was used for validation of the phase behavior. A sample loop, with a measured volume of 0.47 cm^3, was fashioned from 316-stainless steel tubing (also 2.5 mm i.d.) and used to collect samples. Samples from the reactor were isolated and analyzed for either octane (GC) or potassium nitrate (HPLC). The concentration of tracer compound in this sample (C_S) was then related to the volume fraction of the dispersed phase (ϕ_D) by assuming quantitative partitioning of the entire mass of chemical tracer into the dispersed phase.

Volume fractions of the dispersed water and carbon dioxide phases were measured at acoustic power densities up to 0.6 W/cm^3. For both emulsions, the concentration of the dispersed phase increased with power density until a saturation condition was reached at roughly 0.5 W/cm^3; further increases of the power density had little effect on the concentration of the dispersed phase. The volume fractions of dispersed phases present at saturation conditions were 0.05 ± 0.01 for the carbon dioxide droplets in the carbon dioxide/water emulsion (referred to as $\phi_{D,C}$) and 0.10 ± 0.02 for the water droplets in the water/carbon dioxide emulsion (referred to as $\phi_{D,W}$).

Droplet sizing

A novel high-pressure microreactor, designed and constructed by members of K. F. Jensen's research group at M.I.T., was used as a view cell for imaging emulsion droplets. The microreactor consists of a silicon slab (315 mm long $\times$ 10.3 mm wide $\times$ 1 mm thick) in which a narrow channel (200 mm long $\times$ 0.625 mm wide $\times$ 0.250 mm deep) has been etched using a standard SF_6 treatment (Deep Reactive Ion Etch, Surface Technology Systems). The channel is sealed by a pyrex window that is attached to the silicon by a conventional anodic bond. The pressure connections are a technical innovation that will be described in greater detail in a forthcoming report. The microdevice was attached with epoxy to an aluminum chuck for better stability and interfaced with the acoustic reactor via 1/8 in (0.32 cm) o.d. 316-stainless steel tubing. Failure testing of the microdevice indicated a maximum operating pressure of roughly 130 bar (at 25°C), though this could be improved by increasing the thickness of the pyrex window.

Emulsion samples were imaged *in situ* by means of video-enhanced microscopy (Zeiss Axiovert 200). The resolution of the microscope was 0.29 μm/pixel, which allowed features larger than about 1 μm to be resolved. The accuracy of the microscope was verified by polystyrene latex calibration standards (Duke Scientific) with average diameters of 4 and 20 μm. To determine droplet size distributions, digital images were analyzed both manually and by using commercially available software (ImageJ, made available free of charge at http://rsb.info.nih.gov/ij/ by NIH). In all, 6 experiments were conducted and roughly 400 droplets were imaged and analyzed in each experiment. This sample size is sufficient for statistical analysis.

Emulsions were formed by the procedure described above (30°C, 80 bar, 0.6 W/cm^3, 20 kHz, 2 min sonic irradiation, 25% duty of a 1 s cycle) and were sampled directly following termination of sonication. The sampling technique was identi-

cal to that used to measure the concentrations of the dispersed phase. Droplet size distributions were roughly log-normal. The average (volume/surface area) droplet diameters (d_{32}, i.e., the Sauter diameter) were determined directly from the images and were found to be 9.1 μm (statistical FWHM = 6 μm) for water droplets in the water/carbon dioxide emulsion and 15.1 μm (statistical FWHM = 10 μm) for the carbon dioxide droplets in the carbon dioxide/water emulsion. The accuracy of these values is discussed below.

Because there was a 3-5 minute delay between obtaining a sample and analyzing it, droplets were imaged after they had become attached to either the silicon or pyrex surfaces. Some droplet spreading on these surfaces was anticipated, and attempts were made to correct for this error. The contact angles of water and perfluorohexane (our simulant for dense carbon dioxide) droplets were measured on the silicon surface, and these experiments suggested that the surface was hydrophilic. Thus, spreading of the hydrophobic carbon dioxide droplets was probably small and, for the carbon dioxide droplets, the measured image diameter is likely within 10% of the actual diameter.

Water droplets are expected to spread significantly on the hydrophilic surfaces, which had presumably become partially oxidized to silica upon contact with atmospheric oxygen. As a consequence of spreading, the actual droplet sizes might be smaller than their image sizes. Based on contact angle measurements for water droplets in a perfluorohexane environment and profiles of water droplets imaged on the silicon walls of the microchannel in a pressurized carbon dioxide atmosphere, we estimate a lower limit for the average water droplet diameter to be roughly 2 μm—more than four times smaller than that obtained directly from the images. Known de-emulsification times are inconsistent with this figure; given the experimentally observed coagulation times, Smoluchowski theory suggests a droplet diameter on the order of 6 μm. Though we are actively engaged in improving our knowledge of emulsion droplet diameters, the measurements reported here are sufficient for further analysis.

The sizes of carbon dioxide and water droplets obtained using ultrasound are comparable with the larger droplets observed in surfactant-stabilized water/carbon dioxide emulsions,[20] which range from roughly 0.1-10 μm. Although there are no prior data on droplet sizes obtained by sonicating $scCO_2$/water mixtures, ultrasonic emulsification of oil and water[38,39] provides a comparison for our data. Depending on the conditions, ultrasound produces droplets of either oil or water with diameters on the order of 1-10 μm, though formation of droplets as small as 0.2 μm has been reported in some cases.[40,41] The droplet sizes measured here are somewhat larger than those in these two benchmark data sets (that is, [20] and [38-41]), consistent with the fact that we have not used surface-active agents to form or stabilize our emulsions.

Volume fraction measurements ($\phi_{D,C}$ and $\phi_{D,W}$) and droplet diameters ($d_{32,C}$ and $d_{32,W}$) were used to calculate specific interfacial area (either a_{CW} for a carbon dioxide/water emulsion or a_{WC} for a water/carbon dioxide emulsion) from the following expressions:

$$a_{CW} = \frac{6\phi_{D,C}}{d_{32,C}} \tag{1a}$$

Table 1. Summary of Carbon Dioxide/Water and Water/Carbon Dioxide Emulsion Characteristics[a]

Emulsion Type[b]	d_{32} (μm)	ϕ_D (vol%)	a (cm^{-1})	a (m^2/kg)
Carbon dioxide/water	15 ± 3[c]	5 ± 1	200	20
Water/carbon dioxide	9[d]	10 ± 2	660[d]	100[d]

[a]Emulsification conditions: 30°C, 80 bar, 0.6 W/cm^3, 20 kHz, 2 min sonic irradiation, 25% duty of a 1 s cycle.
[b]Both types of emulsions were formed simultaneously using the ultrasound protocol.
[c]The uncertainty cited is based on the half-width of the size distribution.
[d]Further details regarding the accuracy of this measurement are located in the text. If the full spreading correction factor is applied, $d_{32} \sim 2$ μm and $a \sim 3000$ cm^{-1} or 500 m^2/kg.

and

$$a_{WC} = \frac{6\phi_{D,W}}{d_{32,W}} \tag{1b}$$

Based on the values of $\phi_{D,C}$, $\phi_{D,W}$, $d_{32,C}$, and $d_{32,W}$ reported above, the specific interfacial area for the carbon dioxide/water emulsion is 200 cm^{-1} and that of the water/carbon dioxide emulsion is 660 cm^{-1}. Relevant emulsion characteristics are summarized in Table 1. Note that only the upper limit for the water droplet sizes (i.e., that obtained directly from our images) is reported in Table 1.

Hydrolysis of benzoyl halides as a model reaction

The hydrolysis of benzoyl halides was selected as the model reaction for probing reaction/mass transport dynamics in biphasic mixtures of carbon dioxide and water:

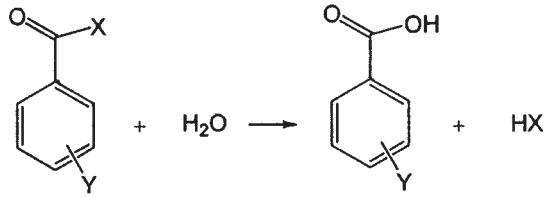

X = F, Cl, Br
Y = H, *o*,*m*,*p*-OCH_3, *p*-NO_2

Our selection of this model system is based on several factors[34]:

(1) Benzoyl halides are virtually water-insoluble but are highly CO_2-soluble.

(2) Hydrolysis of benzoyl halides is irreversible, greatly facilitating interpretation of kinetic data.

(3) In an aqueous solvent, water is present in excess and the hydrolysis reaction can be treated as first order with respect to the halide.

(4) The second-order hydrolysis reaction rate constant for benzoyl chloride is much smaller in nonpolar solvents, such as tetrahydrofuran,[42] than in water.[43-48]

From (4), we infer that hydrolysis rates will be much slower in $scCO_2$ than in water. A slow second order reaction rate constant in carbon dioxide, combined with the low concentration of water in the carbon dioxide phase (roughly 0.05 mol/L

Table 2. Hydrolysis Rate Constants in Pure Water ($k_{r\times n}$) and Estimated Water/Carbon Dioxide Partition Coefficients (K_{CW}) for Model Benzoyl Halides

Benzoyl Halide	K_{CW}[a]	k_{rxn} (s^{-1})	$Ha^b = \sqrt{k_{rxn}D_{AW}}/k_W$	Da_e[c]	k^*_{silent} (s^{-1})	k^*_{sonic} (s^{-1})	$\eta \equiv k^*_{sonic}/k^*_{silent}$
Benzoyl Fluoride	120 ± 30	1.9×10^{-3} [d]	0.5	6×10^{-4}	$1.7 \pm 0.1 \times 10^{-6}$	$7.7 \pm 0.2 \times 10^{-6}$	4.6
p-Nitrobenzoyl Chloride	130 ± 40	0.055[e]	2.4	0.02	$1.7 \pm 0.1 \times 10^{-5}$	$4.6 \pm 0.2 \times 10^{-4}$	30
m-Anisoyl Chloride	220 ± 70	0.6[d]	8.2	0.2	$3.3 \pm 0.3 \times 10^{-6}$	$7.0 \pm 0.4 \times 10^{-4}$	210
Benzoyl Chloride	140 ± 40	1.3[f]	12.0	0.4	$1.1 \pm 0.1 \times 10^{-5}$	$1.8 \pm 0.2 \times 10^{-3}$	160
p-Anisoyl Chloride	220 ± 70	11[g]	35.0	4	$6.5 \pm 0.1 \times 10^{-5}$	$3.6 \pm 0.3 \times 10^{-3}$	60
Benzoyl Bromide	160 ± 50	fast[h]	>35	>4	$1.7 \pm 0.1 \times 10^{-4}$	$3.3 \pm 0.2 \times 10^{-3}$	20
o-Anisoyl Chloride	220 ± 70	fast[h]	>35	>4	$1.1 \pm 0.1 \times 10^{-3}$	0.027 ± 0.002	30

[a]Estimated for experimental conditions using empirical correlations presented in reference [49].
[b]Water-film Hatta number, *Ha,* based on $k_W = 3 \times 10^{-4}$ cm/s and $D_{AW} = 1 \times 10^{-5}$ cm^2/s.
[c]Da_e is the emulsion-based Damköhler number, defined by Eq. 15 in the text.
[d]From reference [44].
[e]From references [44] and [45].
[f]From references [43–48].
[g]From reference [45].
[h]Hydrolysis reaction is too fast to be measured using standard stop-flow techniques.

at 30°C and 80 bar), was expected to confine the reaction primarily to the water phase. Therefore, mass transport of the halide from the carbon dioxide phase to the water phase should be rate determining, as desired.

A further advantage of reaction (A) is that its reaction rate constant in pure water, k_{rxn}, can be varied dramatically by changing the halide leaving group (X) and/or the substituent Y. Table 2 lists values of k_{rxn} for a variety of benzoyl halides and shows a variation over at least 4 orders of magnitude. The most reactive halides (such as benzoyl bromide and *o*–anisoyl halide) hydrolyze too rapidly in pure water for accurate measurement of k_{rxn}, even when sophisticated stop-flow methods are used.

From empirical estimation methods developed earlier in our group,[49] partition coefficients (K_{CW}) are expected to be narrowly distributed. An average value of roughly 150 was estimated based on predictions for 7 different benzoyl halides. Based on reported values of the diffusivities of aromatic molecules at 30°C and 80 bar, we have taken the diffusion coefficient of benzoyl halides in water (D_{AW}) to be 1×10^{-5} cm^2/s.[50-62] Similarly, the diffusivity of benzoyl halides in carbon dioxide (D_{AC}) was taken to be 1×10^{-4} cm^2/s.[63-69]

Kinetic measurements

For batch-wise kinetic studies, the acoustic reactor was partially filled with 40 cm^3 of deionized water and pressurized to 65 bar at 30°C under a carbon dioxide atmosphere. Phase equilibrium was achieved after several hours with the water phase recirculating at a flow rate of 20 cm^3/min. For recirculation, the withdrawal point within the reactor was 5 cm removed from the interface, and the re-injection point was 1 cm from the interface. The recirculating stream was directed through an HPLC valve (Valco Instrument Company, Inc. uw-type) from which water phase samples were taken from the system.

To initiate the reaction, a known quantity of the halide reactant (between 5×10^{-6} and 1×10^{-4} mol) was injected into the reactor as the carbon dioxide pressure was increased to 80 bar. The corresponding initial concentrations of halide in the carbon dioxide phase ranged between 0.1 and 20 mmol/L. Water was always the excess reagent, by a factor of at least 2,000. Visual inspection through the windows of the reactor verified that experiments were conducted under two-phase conditions.

Samples withdrawn from the aqueous phase were analyzed for the corresponding benzoic acid derivative. The analysis was conducted by either GC (Agilent, 6890), equipped with a SPB–5 column (Supelco) and a flame-ionization detector (FID), or by ultraviolet (UV) absorption at roughly 280 nm (Varian, Cary 50). GC was used to analyze samples from experiments with benzoyl fluoride, chloride, and bromide. No byproducts were detected by GC, and only acid and water were present in samples withdrawn from the reactor. Rates measured for benzoyl chloride hydrolysis, on the basis of parallel chemical analysis by the GC and UV techniques, agreed with one another to within ±5%.

The measured concentration of acid in the water phase was used to determine the concentration of unreacted halide by a mole balance, assuming the stoichiometry of reaction (A):

$$n_{halide,CO2}(t) = n_{halide,CO2}(t=0) - n_{acid,water}(t) \qquad (2)$$

where $_{ni,j}$ is the number of moles of compound *i* in phase *j*. In formulating Eq. 2 we have assumed that the concentration of acid in the carbon dioxide phase and the concentration of halide in the water phase are each negligible. Based on the values of the partition coefficient reported for benzoic acid,[70] the former assumption is true to within 10%, while the estimated partition coefficient of benzoyl halides indicates that the latter is true to within 1% (see Table 2). Partitioning of benzoic acid into the carbon dioxide phase limited data analysis to conversions less than 90%. For data collected at conversions below 90%, some of the raw data were corrected by assuming equilibrium partitioning of the benzoic acid between the carbon dioxide and water phases. The correction to measured values of the apparent reaction rate constant was found to be less than 15% in all cases. Here we report kinetic data that have not been corrected for partitioning of benzoic acid.

During each experiment, 2 to 5 samples were withdrawn from the reactor at known time intervals, analyzed for acid content, and the corresponding amount of halide present was determined from Eq. 2. At the end of the run, the contents of

the reactor were collected, mixed with water to complete the reaction, and analyzed for the acid product. Mass balance closure was complete to within ±5% on average and within 15% in the worst case.

Previous research in our group has indicated that increasing the acoustic power density beyond 0.5 W/cm^3 does not appreciably accelerate the hydrolysis rate of benzoyl chloride.[34] In accord with this finding, kinetic data reported here were obtained at a power density of 0.6 W/cm^3. Other conditions were: 30°C, 80 bar, 20 kHz, 25% duty on a 1 s cycle, 40 cm^3 water loading, 2-cm standoff distance between the sonic horn tip and the carbon dioxide/water interface. Although near-critical conditions were selected for these experiments, our experience suggests that power ultrasound should be an effective emulsification method for temperatures and pressures well into the supercritical region.

Mass transport experiments

The mass transfer coefficient for transport from the carbon dioxide phase to the water phase was measured in the absence of either chemical reaction or sonication by using benzaldehyde as a tracer. Benzaldehyde was selected for these experiments because its partition coefficient is well known[49,71] and because its physicochemical properties were expected to be similar to those of the benzoyl halides. Mass transport experiments were conducted using the protocol and conditions described for kinetic measurements. Raw data from the mass transport experiments were analyzed using the two-film model.[72] From these experiments, we concluded that mass transport of hydrophobic solutes is dominated by water side resistance and that the appropriate water side mass transfer coefficient, k_W, was roughly $3.0 \pm 0.6 \times 10^{-4}$ cm/s for our reactor geometry. The mass transfer coefficient on the carbon dioxide side, k_C, is greater than k_W by roughly an order of magnitude.

Although mechanical impellers could be used to achieve much more turbulent mixing (and consequently larger values of k_W) than is possible by using either recirculation pumps or stir bars, we did not explore the use of impellers experimentally in this study. We return to the possible effects of impeller agitation on k_W in the Discussion section.

Theoretical: Model Development

Silent model

A model for the disappearance of benzoyl halide from the carbon dioxide phase was developed to describe global kinetics measured under silent, biphasic conditions. The two-film mass transport model was modified to account for reaction enhancement.[73,74] The transient mass balance equations are:

$$\frac{d[\mathrm{A}]_C}{dt} = -\frac{\underline{a}}{\underline{V}_C}\frac{[\mathrm{A}]_C - \dfrac{K_{CW}[\mathrm{A}]_W}{\cosh(Ha)}}{\dfrac{K_{CW}}{k_W}\dfrac{\tanh(Ha)}{Ha}} \tag{4}$$

and

$$\frac{d[\mathrm{A}]_w}{dt} = -\frac{Ha}{\tanh(Ha)}\frac{\underline{a}}{\underline{V}_W}k_W\left([\mathrm{A}]_W - \frac{[\mathrm{A}]_C}{K_{CW}\cosh(Ha)}\right) - k_{rxn}[\mathrm{A}]_W \tag{5}$$

Ha is sometimes referred to as the Hatta number, which is defined here as:

$$Ha = \frac{\sqrt{D_{AW}k_{rxn}}}{k_w} \tag{6}$$

$[A]_C$ and $[A]_W$ are the concentrations of reactant in the bulk carbon dioxide and water phases, respectively; a is the nominal carbon dioxide/water interfacial area; and $\underline{V}_C$ and $\underline{V}_W$ are the total volumes of the carbon dioxide and water phases. At time equal to zero, $[A]_C = [A]_{C,0}$ and $[A]_W = 0$. Eqs. 4 and 5 incorporate the following assumptions:

(1) The concentration profile of benzoyl halide in the water film is assumed to be quasi-steady. This assumption requires that either $k_{rxn}\, t \gg 1$ [a reaction time scale appropriate for $(D_{AW}\, k_{rxn}) / k_W^2 < 1$] or $(k_W^2 t) / D_{AW} \gg 1$ [a diffusion time scale appropriate for $(D_{AW}\, k_{rxn}) / k_W^2 > 1$]. If the experimentally measured half-lives are used as the characteristic times, $k_{rxn}\, t \gg 100$ (considering halides for which we have accurate values of k_{rxn}) and $(k_W^2 t) / D_{AW} > 100$, so both criteria for quasi-steady conditions in the reaction film are readily satisfied.

(2) All of the resistance to mass transport is assumed to be in the water film. This assumption should be valid provided that $[k_C\, K_{CW} \tanh(Ha)] / (k_W\, Ha) \gg 1$. For our experiments, $(k_C K_{CW})/k_W \approx 10^3$ and $Ha < 50$ (see Table 2), so this condition is easily satisfied.

(3) The reaction can take place only in the water film or in the bulk water phase. Due to the low solubility of water in $scCO_2$ and the influence of solvent polarity on benzoyl halide hydrolysis, this is a reasonable first order approximation. The topic is revisited in the Results section.

An approximate solution to Eqs. 4 and 5, valid for $Ha \geq 0.1$ as it always was in this study, is:

$$\ln\left(\frac{[\mathrm{A}]_C}{[\mathrm{A}]_{C,0}}\right) = -\left[1 - \frac{\dfrac{1}{4} + K_{CW}\dfrac{\underline{V}_C}{\underline{V}_W}\dfrac{1}{\cosh^2(Ha)}}{K_{CW}\dfrac{\underline{V}_C}{\underline{V}_W} + k_{rxn}\tau_{2P}}\right]\frac{t}{\tau_{2P}} \tag{7}$$

where τ_{2P} is given by:

$$\tau_{2P} \equiv \frac{\underline{V}_C}{\underline{a}}\frac{K_{CW}}{k_W}\frac{\tanh(Ha)}{Ha} \tag{8}$$

Equation 7 predicts global first order behavior with respect to the halide reactant.

Emulsion model

The emulsion model is considerably complicated by the simultaneous presence of both carbon dioxide/water and water/carbon dioxide emulsions in our reactor. Nonetheless, a simple model was derived, based primarily on the rate of consumption of reactant in the water droplets and in the bulk water phase. The set of governing equations has a form similar to that for the silent model:

$$\frac{d[\mathrm{A}]_{\mathrm{C}}}{dt} = -\frac{2D_{\mathrm{AW}}}{d_{32,\mathrm{C}}}\frac{\underline{a}_{\mathrm{CW}}}{\underline{V}_{\mathrm{C}}}\frac{1}{K_{\mathrm{CW}}}([\mathrm{A}]_{\mathrm{C,drop}} - K_{\mathrm{CW}}[\mathrm{A}]_{\mathrm{W}}) - \frac{\phi_{\mathrm{D,W}}k_{\mathrm{rxn}}[\mathrm{A}]_{\mathrm{C}}}{K_{\mathrm{CW}}} \quad (9a)$$

$$\frac{d[\mathrm{A}]_{\mathrm{W}}}{dt} = \frac{2D_{\mathrm{AW}}}{d_{32,\mathrm{C}}}\frac{\underline{a}_{\mathrm{CW}}}{(\underline{V}_{\mathrm{W}} - \phi_{\mathrm{D,W}}\underline{V}_{\mathrm{C}})}\frac{1}{K_{\mathrm{CW}}}([\mathrm{A}]_{\mathrm{C,drop}} - K_{\mathrm{CW}}[\mathrm{A}]_{\mathrm{W}}) - k_{\mathrm{rxn}}[\mathrm{A}]_{\mathrm{W}} \quad (9b)$$

and is subjected to the same initial conditions as before. The first term in Eqs. 9a and 9b corresponds to the diffusion of reactant from the carbon dioxide droplets to the bulk water phase. The final term in Eq. 9a accounts for consumption of reactant in the water droplets, and the final term in Eq. 9b is consumption in the bulk water phase (see below for discussion). In Eq. 9b, the volume of the water droplets in the water/carbon dioxide emulsion ($\phi_{\mathrm{D,W}}\underline{V}_{\mathrm{C}}$) is subtracted from the total water loading of the system ($\underline{V}_{\mathrm{W}}$) to determine the volume of water present in the carbon dioxide/water emulsion.

We have implicitly assumed that the concentration in the water droplets is uniform and equal to $[\mathrm{A}]_{\mathrm{C}}/K_{\mathrm{CW}}$ in Eq. 9. This assumption is valid provided that the Damköhler number for reaction within the water droplets [$Da_{\mathrm{W}} = (k_{\mathrm{rxn}} \cdot d_{32,\mathrm{W}}{}^2)$ / D_{AW}] is small compared to unity. Even taking the largest estimate of $d_{32,\mathrm{W}} = 9$ μm, this condition is satisfied in our experiments. Appendix A outlines a procedure to extend the range of applicability of Eq. 9 for Da_{W} slightly larger than unity.

In Eq. 9, $[\mathrm{A}]_{\mathrm{C,\ drop}}$ refers to the concentration of reactant in the carbon dioxide droplets. The emulsion model cannot be solved without knowledge of this quantity. Physically, when a carbon dioxide droplet is first sheared from its bulk phase, the concentration of reactant in the droplet must equal that in the bulk. As the droplet remains in the water phase, however, it will become depleted in reactant. Eventually, the concentration in the droplet will equal $K_{\mathrm{CW}} \cdot [\mathrm{A}]_{\mathrm{W}}$, as the droplet will reach thermodynamic equilibrium with the bulk water phase. A simple solution to Eq. 9 exists for the limiting condition of zero droplet depletion, that is, $[\mathrm{A}]_{\mathrm{C,drop}} = [\mathrm{A}]_{\mathrm{C}}$:

$$\ln\left(\frac{[\mathrm{A}]_{\mathrm{C}}}{[\mathrm{A}]_{\mathrm{C},0}}\right) = -\frac{1 + \dfrac{\underline{V}_{\mathrm{W,drop}}}{\underline{V}_{\mathrm{W}}}Da_{\mathrm{e}}}{1 + Da_{\mathrm{e}}}\frac{t}{\tau_{\mathrm{WM}}} \quad (10)$$

where $\underline{V}_{\mathrm{W}}$,drop = $(\phi_{\mathrm{D,W}})(\underline{V}_{\mathrm{C}})$, Da_{e} is a type of Damköhler number appropriate for emulsions, which we define as:

$$Da_{\mathrm{e}} = \frac{k_{\mathrm{rxn}}d_{32,\mathrm{C}}(\underline{V}_{\mathrm{W}} - \underline{V}_{\mathrm{W,drop}})}{2D_{\mathrm{AW}}\underline{a}_{\mathrm{CW}}} \quad (11)$$

and τ_{WM} is a time constant corresponding to well mixed conditions (i.e., conditions under which $[\mathrm{A}]_{\mathrm{W}} = [\mathrm{A}]_{\mathrm{C}}/K_{\mathrm{CW}}$ everywhere):

$$\tau_{\mathrm{WM}} = \frac{K_{\mathrm{CW}}\underline{V}_{\mathrm{C}}}{k_{\mathrm{rxn}}\underline{V}_{\mathrm{W}}} \quad (12)$$

Equation 10 is useful only as an heuristic. The degree of reactant depletion depends on the lifetime of the droplets (τ_{LT}) relative to the time scale for depletion. Based on our observations of the time required to form the emulsions, we estimate that τ_{LT} is roughly 10 s. The time scale for reactant depletion (τ_{D}) is given by:

$$\tau_{\mathrm{D}} = \frac{d_{32,\mathrm{C}}^2 K_{\mathrm{CW}}}{12D_{\mathrm{AW}}} \quad (13)$$

For our system, τ_{D} is roughly 3 s. Thus, reactant depletion may be substantial. Our challenge was to derive an expression relating $[\mathrm{A}]_{\mathrm{W}}$, $[\mathrm{A}]_{\mathrm{C}}$, and $[\mathrm{A}]_{\mathrm{C,\ drop}}$. If conditions in the bulk are quasi-steady (see below), a microscopic mass balance can be applied to an isolated carbon dioxide droplet:

$$\frac{d[\mathrm{A}]_{\mathrm{C,drop}}(t)}{dt} = -\frac{12D_{\mathrm{AW}}}{d_{32,\mathrm{C}}^2 K_{\mathrm{CW}}}([\mathrm{A}]_{\mathrm{C,drop}}(t) - K_{\mathrm{CW}}[\mathrm{A}]_{\mathrm{W}}) = -\frac{1}{\tau_{\mathrm{D}}}([\mathrm{A}]_{\mathrm{C,drop}}(t) - K_{\mathrm{CW}}[\mathrm{A}]_{\mathrm{W}}) \quad (14)$$

where τ_{D} is defined by Eq. 13. In Eq. 14, reaction-enhancement of the flux from the carbon dioxide droplets is assumed to be negligible (see assumption #2, below). Solving Eq. 14 for $[\mathrm{A}]_{\mathrm{C,drop}}(t)$ is straightforward. The time-averaged solution resulting from integration of $[\mathrm{A}]_{\mathrm{C,drop}}(t)$ over the interval $0 < t < \tau_{\mathrm{LT}}$ is:

$$\langle[\mathrm{A}]_{\mathrm{C,drop}}\rangle\tau_{\mathrm{LT}} - K_{\mathrm{CW}}[\mathrm{A}]_{\mathrm{W}} = \frac{\tau_{\mathrm{D}}}{\tau_{\mathrm{LT}}}([\mathrm{A}]_{\mathrm{C}} - K_{\mathrm{CW}}[\mathrm{A}]_{\mathrm{W}}) \times [1 - \exp(-\tau_{\mathrm{LT}}/\tau_{\mathrm{D}})] \quad (15)$$

For the quasi-steady microscopic mass balance to apply, $[\mathrm{A}]_{\mathrm{W}}$ must change slowly compared to $[\mathrm{A}]_{\mathrm{C,drop}}$. This criterion is easily met as τ_{LT} is many times less than the overall system time constant [$\tau_{\mathrm{sys}} \approx (k^*_{\mathrm{sonic}})^{-1} > 300$ s].

Only bulk concentrations appear on the right-hand side of Eq. 15. Substitution of the time-averaged value of $[\mathrm{A}]_{\mathrm{C,drop}}$ from Eq. 15 into Eq. 9 yields the following expression:

$$\ln\left(\frac{[\mathrm{A}]_{\mathrm{C}}}{[\mathrm{A}]_{\mathrm{C},0}}\right) = -\left[\frac{1 + \dfrac{\underline{V}_{\mathrm{W,drop}}}{\underline{V}_{\mathrm{W}}}\dfrac{Da_{\mathrm{e}}}{[1 - \exp(-\tau_{\mathrm{LT}}/\tau_{\mathrm{D}})]}\dfrac{\tau_{\mathrm{LT}}}{\tau_{\mathrm{D}}}}{1 + \dfrac{Da_{\mathrm{e}}}{[1 - \exp(-\tau_{\mathrm{LT}}/\tau_{\mathrm{D}})]}\dfrac{\tau_{\mathrm{LT}}}{\tau_{\mathrm{D}}}}\right]\frac{t}{\tau_{\mathrm{WM}}} \quad (16)$$

where all of the parameters retain their previous meanings. It is readily verified that Eq. 16 reduces to:

$$\ln\left(\frac{[\mathrm{A}]_{\mathrm{C}}}{[\mathrm{A}]_{\mathrm{C},0}}\right) = -\frac{t}{\tau_{\mathrm{WM}}} \quad (17)$$

in the limit of infinitely slow reaction rate (i.e., as D_{ae} approaches zero) and to:

$$\ln\left(\frac{[A]_C}{[A]_{C,0}}\right) = -\frac{\underline{V}_{W,drop}}{\underline{V}_W}\frac{t}{\tau_{WM}} = -\frac{\underline{V}_{W,drop}k_{rxn}}{K_{CW}\underline{V}_C}t \qquad (18)$$

as $Da_e \gg 1$. Eq. 18 is anticipated by our assumption, valid for $Da_W < 1$, that the concentration of reactant in the water droplets always equals $[A]_C/K_{CW}$. In contrast, the concentration of reactant in the bulk water phase falls to zero for large Da_e, leaving the bulk water phase unutilized. Under all conditions, the emulsion models predict global first order behavior with respect to the halide reactant ($[A]_C$).

Provided that $Da_W < 1$, Eq. 16 is valid for all values of Da_e, subject to the following reasonable assumptions:

(1) As water droplets coalesce with the bulk water phase, they return benzoyl halide reactant to the bulk phase. Based on several calculations, we have ignored this additional flow of reactant to the bulk water phase in Eq. 9. If, as before, the concentration of halide in the water droplets is $[A]_C / K_{CW}$, the flow of reactant to the bulk water phase ($Q_{convection}$) is:

$$Q_{convection} = \left(\frac{\underline{V}_{W,drop}}{\underline{V}_W}\right)\left(\frac{1}{\tau_{LT}k_{rxn}}\right) \qquad (19a)$$

In Eq. 19a we have assumed that the lifetime of a water droplet equals that of a carbon dioxide droplet (τ_{LT}). The other source of halide flow into the bulk water phase is diffusion from the carbon dioxide droplets. If the concentration of reactant in the bulk water phase is negligible compared to $[A]_C/K_{CW}$, the diffusional flow can be approximated as:

$$Q_{diffusion}([A]_w=0) = \frac{1}{Da_e}\frac{(\underline{V}_W - \underline{V}_{W,drop})}{\underline{V}_W}\frac{\tau_D}{\tau_{LT}}[1 - \exp(-\tau_{LT}/\tau_D)] \qquad (19b)$$

$Q_{diffusion}([A]_W = 0) \gg Q_{convection}$ provided that $\tau_{LT} > 0.5$ s, as is almost certainly the case, thereby justifying our decision to neglect $Q_{convection}$.

(2) The water film surrounding the carbon dioxide droplets is assumed to adjust instantaneously as the droplets enter the water phase. This assumption is justified by the small Damköhler numbers of this water film [$Da_C = (k_{rxn} \cdot d_{32,C}^2)/D_{AB}$] and the large values of τ_D/τ_{LT} that we expect in our system. Small Da_C also implies that reaction enhancement of diffusion from the carbon dioxide droplets is negligible, as we have assumed in Eqs. 9 and 14.

(3) Although sonochemical effects have been observed in some high pressure carbon dioxide systems,[75] ultrasound was assumed to exert purely physical effects.[37,76] This is justified by experiments that we conducted at 80 bar in a water/carbon dioxide environment with a sonochemical probe reaction: oxidation of potassium iodide to iodine. Under these conditions, sonication of potassium iodide did not produce measurable quantities of iodine, an indication that sonochemical effects were negligible.[77-80]

(4) Halide concentration was assumed to be uniform in both the carbon dioxide droplets and the carbon dioxide continuous phase. This follows directly from the fact that the water phase mass-transfer resistance is 1,000-fold greater than that of the carbon dioxide phase (based on the relative diffusion coefficients of organic solutes in the two phases and their partition coefficients).

(5) The interdroplet distance was assumed to be so large that the droplets behave as if they were at infinite separation. In the water continuous phase, the error introduced by this assumption is minor since the estimated interdroplet distance is 2.5 times the average droplet radius. For the carbon dioxide continuous phase, the interdroplet distance is 1.5 times the average droplet radius, and treating the droplets as if they were at infinite separation is not valid. However, since we have already assumed that the carbon dioxide bulk phase poses no resistance to mass transfer, this is of no consequence.

(6) Convective mass transport to the droplets was assumed to be negligible.[81] The terminal velocity (U_t) of a carbon dioxide droplet rising through the water phase[82] is roughly 4×10^{-3} cm/s, corresponding to a Peclet number [$Pe = (U_t d_{32,C}) / D_{AW}$] of 0.4. For $Pe = 0.4$, Acrivos and Taylor[81] indicate that the convective correction should be small (slightly more than 10%).

Results

The hydrolysis rates of the 7 halides listed in Table 2 were measured under both silent and sonicated conditions (0.6 W/cm^3, 20 kHz, 25% duty of a 1 s cycle) at 30°C and 80 bar. Figure 2 shows raw data from (a) silent and (b) sonicated kinetic runs. In all cases, first order plots were linear ($r^2 > 0.95$). The best fit slopes are listed in Table 2 as k^*_{silent} and k^*_{sonic}, for silent and sonicated conditions, along with statistically based errors (95% confidence limits). Taking into account all possible sources of experimental error, the accuracy of the kinetic measurements is roughly ±20%.

Table 2 shows that both k^*_{silent} and k^*_{sonic} are functions of k_{rxn} over its entire range, suggesting that the intrinsic rate of chemical reaction always contributes to the global rate constant. In all cases, k^*_{silent} is less than k^*_{sonic}, indicating that ultrasound accelerates the overall reaction rate. A sonic enhancement factor, $\eta \equiv k^*_{sonic} / k^*_{silent}$ quantifies this effect: for benzoyl fluoride $\eta < 10$, for more reactive halides, such as benzoyl chloride and *m*-anisoyl chloride, $\eta > 100$. Interestingly, benzoyl bromide and *o*-anisoyl chloride, the most reactive compounds studied, are accelerated only modestly ($\eta \approx 20$).

Effect of mixing and sampling position

Hydrolysis of benzoyl chloride was used as a test case for the effect of mechanical agitation on the observed reaction rate. Both recirculation of the water phase (at 20 mL/min) and stirring with a Teflon-coated stir bar (at roughly 100 rpm) were used as agitation methods. Neither method altered the hydrolysis rate, as compared to that measured under quiescent conditions. In a similar set of experiments, the hydrolysis rate of benzoyl chloride was measured by sampling the water phase from two different positions, either 1 or 5 cm removed from the carbon dioxide/water interface. The hydrolysis rate constants measured by sampling at these two positions were identical within the limits of experimental accuracy. These experiments indicate that the majority of the water phase is well mixed with respect to the product. The rate constants reported in Table 2 were

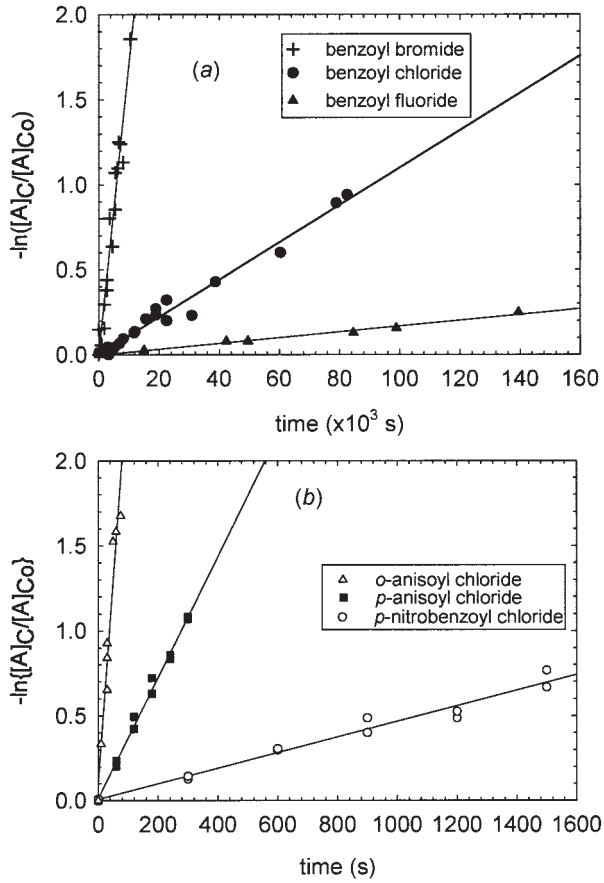

Figure 2. Representative first order plots for benzoyl halide hydrolysis in carbon dioxide/water mixtures under (a) silent conditions and (b) sonicated conditions.

$[A]_C$ and $[A]_{C0}$ are the instantaneous and initial concentrations of benzoyl halide in the carbon dioxide phase, respectively. Conditions: 30°C, 80 bar, 45% water by volume. Ultrasound pulsed at 25% of a 1 s cycle, 20 kHz frequency, 0.60 W/cm^3 volume-averaged power density. The slopes of these plots were taken to be k^*_{silent} and k^*_{sonic}, as listed in Table 2.

measured under conditions of water phase recirculation and with a sampling position 1 cm away from the interface.

Effect of initial concentration

The initial concentration of benzoyl halide reactant was varied in several experiments to determine its effect on observed hydrolysis rates. For an initial benzoyl bromide concentration of either 9 or 18 mM (based on the carbon dioxide phase), the global rate constant measured under silent conditions was $1.7 \pm 0.2 \times 10^{-4}$ s^{-1}. As an example of the effect of concentration on observed kinetics measured during sonication, the global rate constant for *o*–anisoyl chloride was $3.8 \pm 0.5 \times 10^{-3}$ s^{-1} when the initial reactant concentration was equal to 1.6 mM and $3.5 \pm 0.3 \times 10^{-3}$ s^{-1} when the initial reactant concentration was 0.8 mM. The negligible effects of reactant concentration on global rate constants confirms our hypothesis that the overall process is first order with respect to benzoyl halide over the 2-fold range of concentration considered here.

Validation of the silent model

Equation 7 correctly predicts the first order behavior that is observed, and provides theoretical predictions for comparison with experimental data. Figure 3 is a plot of measured hydrolysis rate constants (k^*_{silent}) as a function of *Ha*. The factor τ_{2P} (i.e., the time constant predicted when the concentration of reactant in the bulk water phase is zero) is used to normalize the rate constants plotted in Figure 3. Parameter values used for calculations of *Ha* and τ_{2P} are provided in Table 3. Error bars in Figure 3 are based solely on the uncertainty in the estimated values of K_{CW}, the least accurate parameter in τ_{2P}. The solid line is the prediction of Eq. 7. The normalized prediction is equal to unity for $Ha > 0.5$; for smaller *Ha*, the effect of $[A]_W \neq 0$ becomes important, and the normalized prediction is less than unity. Overall, the predictions agree with the experimental data to within the estimated experimental uncertainty. The most striking outlier in Figure 3 is *p*–nitrobenzoyl chloride (which appears at $Ha = 2.4$), which is underpredicted by a factor of 6. At least part of the discrepancy may be due to an overestimate of the partition coefficient for *p*–nitrobenzoyl chloride (see *Validation of the Emulsion Model* for more discussion).

A likely explanation for the discrepancy observed for $Ha > 20$ is that hydrolysis of highly reactive benzoyl halides may occur appreciably in both the carbon dioxide and the water phases, which implies that diffusion in the water phase may no longer be the rate determining step. A simple calculation confirms this possibility. The equilibrium concentration of water in carbon dioxide (roughly 0.1 mol/L at 30°C and 80 bar[15]) is 10-fold greater than the initial concentration of the organic reactant. This concentration results in a pseudo-first order reaction rate constant in carbon dioxide that is smaller than that

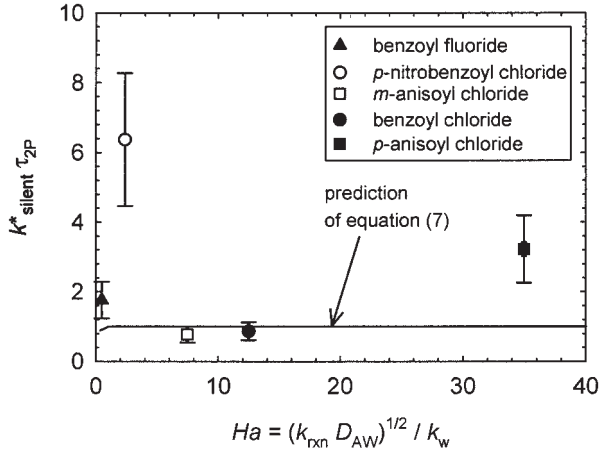

Figure 3. Measured rate constants for benzoyl halide hydrolysis under silent conditions (k^*_{silent}) normalized by $\tau_{2P} = [V_C K_{CW} \tanh(Ha)] / (a k_W Ha)$ plotted versus the water film Hatta number, $Ha = (k_{rxn} D_{AW})^{1/2} / k_w$.

The solid line is a prediction of $k^*_{silent}\ \tau_{2P}$ based on Eq. 7. The prediction deviates slightly from unity for $Ha \ll 1$. Raw data are presented in Table 2.

Table 3. Values of Physical Parameters Appearing in Eqs. 7 and 8

Physical Description	Variable	Value
Waterfilm mass transport coefficient	k_W	3×10^{-4} cm/s
First order rate constant in pure water	k_{rxn}	2×10^{-3} to 11 s^{-1}
Waterfilm Hatta number	$Ha = \sqrt{k_{rxn} D_{AW}}/k_w$	0.5 to 35
Diffusivity of organic solute in water	D_{AW}	1×10^{-5} cm^2/s
Interfacial area	a	20 cm^2
Total volume of water phase	V_W	40 cm^3
Total volume of carbon dioxide phase	V_C	47 cm^3
Partition coefficient	$K_{CW} = \frac{C_{CO_2}}{C_{H_2O}}$	150

in water by about a factor of 10^6. For benzoyl chloride, the rate of reaction-enhanced mass transport predicted by Eq. 7 is 10-fold greater than the hydrolysis rate predicted in the carbon dioxide phase. This implies that reaction in the carbon dioxide phase should be a negligible pathway for benzoyl chloride; hence, the good agreement between the model and this data point is expected.

However, for compounds more reactive than benzoyl chloride, this argument is no longer tenable, because reaction in the carbon dioxide phase increases as the first power of k_{rxn} whereas that in the water phase increases roughly as the square root of k_{rxn}. Specifically, the hydrolysis rate in the carbon dioxide phase and the transport rate to the water phase are essentially equal for $Ha \approx 100$ ($k_{rxn} \approx 100$ s^{-1}). Thus, as the intrinsic reactivity of the halides increases, the relative importance of hydrolysis in the carbon dioxide phase also increases. It seems likely that benzoyl bromide and *o*–anisoyl chloride are so reactive that the carbon dioxide pathway is quite important. The 3-fold underprediction of the data point appearing at $Ha \approx 36$ (i.e., *p*-anisoyl chloride) is qualitatively consistent with the relative importance of a carbon dioxide phase reaction increasing with *Ha*, as we hypothesize.

Validation of the emulsion model

As for the silent case, the emulsion model correctly predicts the global first order behavior that was observed experimentally, thus encouraging a direct comparison between predictions and data. Figure 4 is a plot of k^*_{sonic} normalized by τ_{WM} as a function of $(Da_e)^{1/2}$. $(Da_e)^{1/2}$ was selected by direct analogy to the analysis of the silent data set, for which *Ha* (which also scales with the square root of k_{rxn}) served as the plotting variable. As before, error bars in Figure 4 are based entirely on uncertainties in K_{CW}. Parameter values used for predictions of k^*_{sonic} are provided in Table 4. Predictions based on Eq. 10 (i.e., $\tau_{LT} / \tau_D = 0$) are shown along with those of Eq. 16 for $\tau_{LT} / \tau_D = 3$, 10, 30, and approaching ∞. For $\tau_{LT} / \tau_D = 0$, the normalized predictions of k^*_{sonic} are in good qualitative agreement with the data; quantitatively, the predictions agree with the data to within a factor of 4 in the worst case ($Da_e^{1/2} \approx 1.7$).

The good general agreement notwithstanding, the predictions of Eq. 10 are systematically too high. Overprediction of the reaction rate constant is consistent with a lifetime of the carbon dioxide droplets that is greater than the depletion time scale. Although the quality of the experimental data set is insufficient to unambiguously determine a value for τ_{LT}, a lifetime on the order of 10 s (i.e., $\tau_{LT} / \tau_D \approx 3$) provides good agreement with the available data and is entirely consistent with our independent observations of emulsification times.

As τ_{LT} / τ_D increases from zero to modest values, the drops become increasingly depleted in halide, thus leading to lower values of k^*_{sonic}. This behavior is expected. However, one might expect the dependence on τ_{LT} / τ_D to saturate for droplet lifetimes roughly 3-fold greater than τ_D. After all, if τ_{LT} / τ_D is greater than roughly 3, the droplets are entirely depleted of reactant (up to that allowed by equilibrium constraints) prior to their return to the carbon dioxide phase. Thus, one might expect that droplet lifetime should not affect predictions of k^*_{sonic} provided that $\tau_{LT} / \tau_D > 3$. By this logic, one expects that the predicted curves shown in Figure 4 should be completely superimposed in the long droplet lifetime regime. Instead, the model predictions show a clear dependence on droplet lifetime for all values of τ_{LT} / τ_D between zero and infinity, a result that is surprising at first consideration.

The resolution of this apparent paradox requires that one be very careful about specifying exactly what is held constant in order to vary τ_{LT} / τ_D. If everything is held constant except D_{AW}, which is imagined to increase, then both τ_{LT} / τ_D and Da_e will change. For instance, if τ_{LT} / τ_D changes from 3 to 10 due

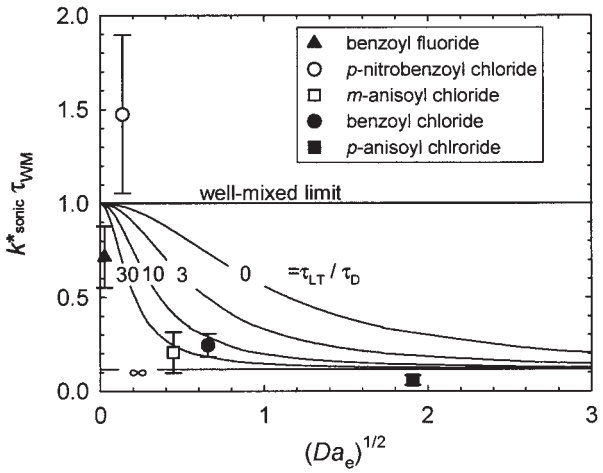

Figure 4. Measured hydrolysis rates under sonic conditions, k^*_{sonic}, normalized by τ_{WM}, plotted vs. the square root of the emulsion-based Damköhler number (Da_e).

Da_e is defined by Eq. 11 in the text, while τ_{WM} is defined by Eq. 12. The horizontal line is the prediction for well mixed conditions. The remaining lines are the predictions of Eq. 10 for $\tau_{LT} / \tau_D = 0$ and of Eq. 16 for $\tau_{LT} / \tau_D = 3$, 10, 30, and approaching ∞. Raw data are presented in Table 2. Conditions: 30°C, 80 bar, 45% water by volume. Ultrasound pulsed at 25% of a 1 s cycle, 20 kHz frequency, 0.60 W/cm^3 volume-averaged power density.

Table 4. Values of Physical Parameters Appearing in Eq. 9

Physical Description	Variable	Value
Diffusivity of organic solute in water	D_{AW}	1×10^{-5} cm^2/s
First order rate constant in pure water	$k_{r\times n}$	1×10^{-5} to 10 s^{-1}
Interfacial area in CO_2/H_2O emulsion	a_{CW}	7,000 cm^2
Total volume of water phase	$\underline{V}_W$	40 cm^3
Total volume of carbon dioxide phase	$\underline{V}_C$	47 cm^3
Volume of fraction of water phase Water/carbon dioxide emulsion	$\phi_{D,W}$	0.1
Diameter of a carbon dioxide droplet	$d_{32,C}$	15.1 μm
Partition coefficient	$K_{CW} = \frac{C_{CO_2}}{C_{H_2O}}$	150

to a change in D_{AW}, then $(Da_e)^{1/2}$ will diminish by a factor of 1.8. Figure 4 then shows that the consequence is essentially no change in k^*_{sonic}—just as was expected. Conversely, if all of the parameters in τ_D are held constant, but τ_{LT} is imagined to increase with ϕ_{CW} still held constant, this requires that k^*_{sonic} decrease. This too is unsurprising because varying τ_{LT} while holding all other parameters constant implies that the volumetric rate of droplet generation has decreased. As τ_{LT} / τ_D approaches infinity, then either the transport of halide from the carbon dioxide droplets (if D_{AW} is imagined to vary) or the volumetric rate of droplet generation (if τ_{LT} is imagined to vary) is zero. The horizontal line in Figure 4 corresponds solely to consumption of halide in the water droplets, with no contribution from the carbon dioxide/water emulsion. Thus, predictions of k^*_{sonic} should depend on τ_{LT} / τ_D over its entire range, as is shown in Figure 4.

The data point for *p*–nitrobenzoyl chloride, plotted at $(Da_e)^{1/2} \approx 0.1$, is an outlier from the remaining data set by about a factor of 3 and is likewise underpredicted by the models. Similarly, the global hydrolysis rate of *p*–nitrobenzoyl chloride is underpredicted in the silent case by a factor of 6. Uncertainties in the model parameters (see Tables 3 and 4) are a major source of error in the model predictions and come under scrutiny for *p*–nitrobenzoyl chloride. The value for k_{rxn} used in the predictions is not suspect as two separate groups report values for this hydrolysis reaction rate constant,[44,45] the values of which agree to within 10%. However, 3-fold overprediction of the *p*–nitrobenzoyl chloride partition coefficient is within the accuracy of the empirical correlation used to estimate K_{CW}[49] and would largely explain the discrepancy between the model and the data point in question.

The issue of parameter uncertainty warrants further examination, and we have used benzoyl chloride as a test case. In Tables 1 and 2, we provide estimates of the uncertainties for most of the variables that appear in Eqs. 12, 13, and 16; in addition, we assumed ±30% accuracy for k_{rxn} (based on the variability in the 5 reported values), ±20% accuracy for D_{AW}, and that K_{CW} was between 100 and 200, based on the uncertainty inherent to the best available correlation methods.[49] If there is no cancellation of errors among the uncertainties in the various parameters (i.e., the extreme values of the parameters are used to calculate the largest and smallest possible values of k^*_{sonic}), k^*_{sonic} ranges over a full order of magnitude—from 1×10^{-3} to 1×10^{-2} s^{-1}. Nearly 75% of the error is contained in the uncertainty of the partition coefficient. A much more conservative method for estimating the error is to propagate the uncertainties (see Appendix B for details) in the various physical parameters through Eqs. 12, 13, and 16. The calculated range of values for k^*_{sonic} is then 2×10^{-3} to 6×10^{-3} s^{-1}. Thus, the discrepancy between calculated and measured kinetic parameters can largely be attributed to uncertainty in the various parameters, especially K_{CW}.

As in the silent case, hydrolysis in the carbon dioxide phase may be introduced as an additional pathway in Eq. 9, but the predictions are not altered. This is a consequence of the fast transport of benzoyl halide to the water phase under sonicated conditions.

Discussion

We address three outstanding issues in this section: (1) the relative importance of the carbon dioxide/water versus water/carbon dioxide emulsion as a function of Da_e, (2) comparison of ultrasonic mixing with impeller agitation, and (3) the expectations for using the acoustic reactor for large-scale processes.

Because ultrasound generates both carbon dioxide/water and water/carbon dioxide emulsions, a natural question is: Which of the two emulsions dominates the global conversion rate? This question can be answered by consideration of Eq. 16 and Figure 4. For $Da_e \ll 1$, Eq. 16 shows that the global rate constant equals $1/\tau_{WM}$. Thus, at small Da_e we expect that $k^*_{sonic} \cdot \tau_{WM}$ should equal unity, as is shown in Figure 4. Physically, this implies that all of the water contained in the reactor is fully utilized and $[A]_W = [A]_C/K_{CW}$ everywhere. In our system, the majority of the water resides in the carbon dioxide/water emulsion. Thus, for small Da_e, the global rate constant is determined primarily by the carbon dioxide/water emulsion by the factor $(\underline{V}_W - \underline{V}_{W,drop})/\underline{V}_{W,drop} \approx 8.5$. On the other hand, for $Da_e \gg 1$, Eq. 18 applies and the global rate constant reduces to $(k_{rxn}\ \underline{V}_{W,drop}) / (K_{CW}\ \underline{V}_C)$. At this extreme, the water contained in the carbon dioxide/water emulsion is not utilized at all and the global rate constant is determined entirely by the water/carbon dioxide emulsion. In Figure 4, predictions of k^*_{sonic} approach $(k_{rxn}\ \underline{V}_{W,drop}) / (K_{CW}\ \underline{V}_C)$ for large Da_e, as expected.

For intermediate Da_e, the concentration of halide in the bulk water phase is neither zero nor equal to $[A]_C/K_{CW}$. Thus, the rate constant is expected to lie between $(k_{rxn}\ \underline{V}_W) / (K_{CW}\ \underline{V}_C)$ and $(k_{rxn}\ \underline{V}_{W,drop}) / (K_{CW}\ \underline{V}_C)$, as is shown in Figure 4. This effect can easily be quantified by solving Eq. 9 for $[A]_W$. Interpretation of $[A]_W$ is easier if the concentration is normalized by $K_{CW} / [A]_C$. The resulting normalized expression is:

$$\frac{K_{CW}[A]_W}{[A]_C} = \frac{1}{1 + Da_e \dfrac{\tau_{LT}}{\tau_D} \dfrac{1}{[1 - \exp(-\tau_{LT}/\tau_D)]}} \approx \frac{1}{1 + Da_e \dfrac{\tau_{LT}}{\tau_D}} \quad (\text{for } \tau_{LT}/\tau_D \geq 3) \quad (20)$$

As expected, $(K_{CW}\,[A]_W)\,/\,[A]_C$ goes to zero for large Da_e as k^*_{sonic} goes to $(k_{rxn}\,\underline{V}_{W,drop})\,/\,(K_{CW}\,\underline{V}_C)$. Depletion decreases the value of Da_e for which k^*_{sonic} begins to approach $(k_{rxn}\,\underline{V}_{W,drop})\,/\,(K_{CW}\,\underline{V}_C)$. As a quantitative example, for $\tau_{LT}\,/\,\tau_D = 3$, $K_{CW}[A]_W$ equals 50% of $[A]_C$ for $(Da_e)^{1/2} \approx 0.6$. Thus, the curve corresponding to $\tau_{LT}\,/\,\tau_D = 3$ in Figure 4 should predict that k^*_{sonic} is roughly midway between $(k_{rxn}\,\underline{V}_W)\,/\,(K_{CW}\,\underline{V}_C)$ and $(k_{rxn}\,\underline{V}_{W,drop})\,/\,(K_{CW}\,\underline{V}_C)$ for $(Da_e)^{1/2} \approx 0.6$, as it is.

From our analysis, a simple interpretation of Figure 4 is possible. The water/carbon dioxide emulsion makes a contribution to k^*_{sonic} equals $(k_{rxn}\,\underline{V}_{W,drop})\,/\,(K_{CW}\,\underline{V}_{W,drop})$ and is constant with respect to Da_e. Thus, the water/carbon dioxide contribution to k^*_{sonic} can be identified as the horizontal line corresponding to $\tau_{LT}\,/\,\tau_D = \infty$. The carbon dioxide/water emulsion is responsible for any contribution to k^*_{sonic} above the water/carbon dioxide horizontal line.

A second natural question to ask is: Under what conditions is power ultrasound preferred over mechanical mixing? Our approach was to determine conditions under which τ_{WM} could be attained for either ultrasonic or mechanical mixing. The premise is that more efficient mixing can be used to accelerate faster reactions to their maximum possible rate, the well mixed limit. In Figure 4 well mixed conditions are approached to within about 20% for $Da_e < 0.03$. For reactions slower than this, sonication in our reactor essentially removes all mass transport barriers, allowing the reaction to proceed with a global time constant equal to τ_{WM}. In more accessible terms, for a reaction that proceeds with a characteristic half life longer than roughly 10 s (i.e., $k_{rxn} < 0.1\ s^{-1}$), we expect it to proceed at the well mixed rate in the biphasic reactor when sonic agitation is applied.

For silent conditions, the modified film-model of Eqs. 4 and 5 predicts that the well mixed limit will be reached for $Ha < 0.03$. $Ha < 0.03$ corresponds to slower reactions than considered here and, accordingly, well mixed conditions were not approached in any of the silent experiments. Since we performed silent experiments with only gentle agitation, it would be more realistic to compare ultrasonic mixing with the mechanical mixing that can be achieved with a high speed impeller. The key parameter in the analysis is the water film mass transport coefficient (k_W). Tai et al.[83] studied mass transport in a phase-separated $scCO_2/H_2O$ system and reported that impeller agitation resulted in a 10-fold increase of the overall mass coefficient, relative to that measured in the unstirred case. This result is consistent with measurements of the effect of mixing on the water-based mass transport coefficient in water/organic systems.[84-86]

If k_W is 10 times the value reported here (i.e., $k_W \approx 3 \times 10^{-3}$ cm/s), only benzoyl fluoride would be expected to approach the well mixed limit in an impeller-agitated, but silent, reactor. Generalizing, mechanical mixing can be expected to accelerate reactions with half lives longer than about 15 min to that expected for well mixed conditions. We note that phase dispersion resulting from impeller agitation would be expected to extend this limit to faster reactions. In any event, ultrasonic mixing has no clear advantage over impeller agitation for reactions with half lives longer than 15 min since both agitation methods provide the well mixed limit. For reactions with half lives less than roughly 15 min, ultrasonic mixing is preferred over impeller agitation.

The third question to be addressed is: Can the acoustic reactor be used for industrial-scale applications, or is it primarily a laboratory-scale tool? Scale-up of sonochemical reactors is a challenging task, and we do not expect that scaling the high-pressure emulsifier to be substantially easier. Typically, studies on the use of ultrasound to promote chemical reactions have been conducted in batch reactors with small volumes (less than 100 cm^3), with small probe tip areas (roughly 1 cm^2), and at acoustic power densities on the order of 1 W/cm^3. Increasing the volumes of sonochemical reactors to the liter scale and beyond is plagued by inefficient penetration of the ultrasound into the bulk of the liquid,[76] but there has been some progress.

Gogate and Pandit[87] note that multiple sonic horns (possibly operating at different frequencies from one another) allow scale-up of sonochemical reactors to roughly 10 L. Destaillats et al.[88] reported the use of a sonochemical reactor with three sonic horns, a working volume of 6 L, and a power input of 3 kW for the degradation of dichloromethane and trichloroethylene. Gogate et al.[89] designed a hexagonal sonochemical reactor with a working volume of 7 L. This reactor was equipped with 18 sonic horns (50 W power output each) set to operate over a range of frequencies (ranging from 20 to 50 kHz). Similar strategies might reasonably be expected to be used for scale-up of the high-pressure emulsifier.

In the meantime, the productivity of the reactor used in this study could be greatly enhanced simply by operating the reactor in a continuous, rather than batch, mode. The time required to form emulsions in the reactor is on the order of 10 s, while the emulsions break in roughly 10 min. This 60-fold difference in time scales suggests a design consisting of a flow-through emulsification section followed by a conventional tubular reactor. Based on the time required to form the emulsions and the volume of the reactor (roughly 100 cm^3), we calculate that roughly 10 cm^3/s of the two fluids can be emulsified with our design. To maintain the dispersion of the carbon dioxide and water phases during their residence in the tubular reactor, their residence times in the silent section must be less than 10 min. Reactions with time constants much less than 10 min ($k^*_{sonic} \gg 2 \times 10^{-3}\ s^{-1}$) can be expected to run to completion in the tubular section. For an initial reactant concentration of 0.10 mol/L, an assumption of complete conversion leads to an overall production rate of nearly 4 mol/hr. For many purposes, this is ample. For reactions that do not run to completion in 10 min, a silent stirred-tank reactor combined with a sonicated recirculation loop is recommended. If the volume of the sonicated zone is roughly 100 cm^3 and the residence time in this zone is to be 10 s, then the volumetric flow rate through the recirculation loop can be up to 10 cm^3/s. At this recirculation rate, the requirement of 10 minutes residence in the silent zone permits the volume of the stirred tank to be as large as 6 L. The production rates possible with this reactor are determined by global kinetics and the volume of the silent, stirred-tank reactor.

The preceding examples maintain the small size of the emulsification section and, therefore, completely avoid the complications associated with inefficient penetration of ultrasound over long distances. However, if the advances reported for sonochemical reactor designs can be applied to the high-pressure emulsification process, we can expect even greater benefits. We will use the 6-liter reactor described by Destaillats et al.[88] as the basis of our calculations. If it is assumed that 10 s are required for emulsification in the 6-liter tank, the maximum

possible flow rate through this volume, consistent with good emulsification, is 600 cm^3/s. The residence time in a tubular reactor located downstream of this emulsification stage must be less than 10 min, as before. For a flow rate of 600 cm^3/s and an initial reactant concentration of 0.10 mol/L, complete conversion in the tubular reactor leads to an overall production rate of more than 200 mol/h. For the combination of a stirred tank reactor and a sonicated recirculation loop, a flow rate of 600 cm^3/s and a residence time equal to 10 minutes gives a reactor volume of roughly 360 L. These scales are certainly sufficient for production of many high value-added products, such as pharmaceuticals and specialty chemicals.

Conclusions

Ultrasound is an effective, surfactant-free means of contacting dense, near-, and supercritical carbon dioxide and water in the form of emulsions. For our system, the measured diameters of both water and carbon dioxide droplets were roughly 10 μm, with dispersed phase volume fractions of 0.05-0.10.

To evaluate the effects of sonication on global reaction rates, the rates of 7 benzoyl halide hydrolysis reactions were measured. This choice of reactions led to a simplified analysis as they were first order with respect to benzoyl halide and irreversible. Furthermore, their rates in pure water are well known, and this eliminates considerable uncertainty from the analysis. Ultrasonic agitation was found to increase hydrolysis rates in all cases, the maximum acceleration exceeding 200-fold. The global kinetics were found to be first order with respect to the benzoyl halide reactant in all cases.

Physical models were developed to describe mass transport/reaction dynamics under silent, biphasic conditions and for the sonicated, emulsified case. Both models correctly predicted global first order behavior. Quantitatively, the experimental data sets agreed well with model predictions. The model for the silent case was based on simple reaction-enhanced mass transport through a stagnant water film. Though the majority of the reaction occurred in the water film under most conditions, the silent model suggested conditions under which reaction of the benzoyl halide in the carbon dioxide phase becomes important. Our analysis also suggests that water-film resistance is the primary barrier to mass transport in biphasic systems consisting of carbon dioxide/water, particularly for hydrophobic solutes.

Because our ultrasound technique simultaneously forms both water/carbon dioxide and carbon dioxide/water emulsions, the emulsion model needed to account for consumption in both the water droplets (in the water/carbon dioxide emulsion) and the bulk water phase of the carbon dioxide/water emulsion. Reactant was transported to the bulk water phase via diffusion from the carbon dioxide droplets. Qualitative trends were correctly predicted by a model that did not allow for depletion of reactant in the carbon dioxide droplets during their residence in the bulk water phase. Accounting for reactant depletion in the carbon dioxide droplets brought predictions into quantitative agreement with the data set. The model also suggested an emulsion-based Damköhler number as a convenient scaling parameter. This Damköhler number was used to identify which emulsion (carbon dioxide/water or water/carbon dioxide) dominated global dynamics. The success of the emulsion model strongly suggests that sonic acceleration is a purely physical phenomenon in our system. The dominant effect of ultrasound is to increase the carbon dioxide/water interfacial area. Two more subtle effects are also important: (1) saturation of the water droplets and (2) reactant depletion in the carbon dioxide droplets.

Acknowledgments

The U.S. Environmental Protection Agency Technology for a Sustainable Environment Program (agreement # R 826738–01–0) and the Cambridge University–MIT Institute provided funding for this research. MTT thanks the Martin family and the Singapore–MIT Alliance for fellowship support. Andrew J. Allen conducted several hydrolysis experiments at room temperature and ambient pressure, and his assistance is acknowledged. The authors thank members of the Tester, Danheiser, Jensen, and Hatton research groups at MIT, and the Holmes research group at Cambridge University for encouragement and helpful discussion. The gracious help of E. R. Murphy (microdevice fabrication) and A. Günther (digitally enhanced microscopy) of the Jensen group at MIT is particularly appreciated.

Literature Cited

1. Tundo P, Anastas PT, eds. *Green Chemistry: Challenging Perspectives.* New York: Oxford University Press; 2000.
2. Anastas PT, Warner JC. *Green Chemistry: Theory and Practice.* New York: Oxford University Press; 1998.
3. Lubineau A, Auge J. Water as a solvent in organic synthesis. *Topics in Current Chemistry*. 1999;206:1-39.
4. Fringuelli F, Piermatti O, Pizzo F, Vaccaro L. Recent advances in Lewis-acid catalyzed Diels-Alder reactions in aqueous media. *Eur J Org Chem*. 2001;3:439-455.
5. Jessop PG, Leitner W. eds., *Chemical Synthesis Using Supercritical Fluids.* New York: Wiley–VCH; 1999.
6. Oakes RS, Clifford AA, Rayner CM. The use of supercritical fluids in synthetic organic chemistry. *J Chem Soc Perkins Trans 1*. 2001;9:917-941.
7. Leitner W. Supercritical carbon dioxide as a green reaction medium for catalysis. *Acc Chem Res*. 2002;35:746-756.
8. Newman DA, Hoefling TA, Beitle RR, Beckman EJ, Enick RM. Phase-behavior of fluoroether-functional amphiphiles in supercritical carbon dioxide. *J Supercrit Fluids*. 1993;6:205-210.
9. McClain JB, Betts DE, Canelas DA, et al. Design of nonionic surfactants for supercritical carbon dioxide. *Science*. 1996;274:2049-2052.
10. Luna–Barcenas G, Mawson S, Takishima S, DeSimone JM, Sanchez IC, Johnston KP. Phase behavior of poly(1,1–dihydroperfluorooctylacrylate) in supercritical carbon dioxide. *Fluid Phase Equil*. 1998;146:325-337.
11. McHugh MA, Krukonis V. *Supercritical Fluid Extraction*. 2nd ed. Boston, MA: Butterworth–Heinemann; 1994.
12. Wiebe R. The binary system carbon dioxide-water under pressure. *Chem Rev*. 1941;29:475-481.
13. Wiebe R, Gaddy VL. Vapor phase composition of carbon dioxide-water mixtures at various temperatures and at pressures to 700 atmospheres. *J Am Chem Soc*. 1941;63:475-477.
14. Wiebe R, Gaddy VL. The solubility in water of carbon dioxide at 50, 75, 100°C, at pressures to 700 atmospheres. *J Am Chem Soc*. 1939;61:315-318.
15. King MB, Mubarak A, Kim JD, Bott TR. The mutual solubilities of water with supercritical carbon dioxide. *J Supercrit Fluids*. 1992;5:296-302.
16. Nolen SA, Lu J, Brown JS, et al. Olefin epoxidations using supercritical carbon dioxide and hydrogen peroxide without added metallic catalysts or peroxy acids. *Ind Eng Chem Res*. 2002;41:316-323.
17. Sarbu T, Styranec T, Beckman EJ. Non-fluorous polymers with very high solubility in supercritical CO_2 down to low pressures. *Nature*. 2000;405:165-168.
18. Eastoe J, Dupont A, Steytler DC. Fluorinated surfactants in supercritical CO_2. *Curr Opin Coll Int Sci*. 2003;8:267-273.
19. Behles JA, DeSimone JM. Developments in CO_2 research. *Pure and Appl Chem*. 2001;73:1281-1285.
20. Dickson JL, Psathas PA, Salinas B, et al. Formation and growth of water-in-CO_2 miniemulsions. *Langmuir*. 2003;19:4895-4904.
21. Eastoe J, Paul A, Nave S, et al. Micellization of hydrocarbon surfac-

tants in supercritical carbon dioxide. *J Am Chem Soc*. 2001;123:988-989.
22. Lee CT, Ryoo W, Smith PG, et al. Carbon dioxide-in-water microemulsions. *J Am Chem Soc*. 2003;125:3181-3189.
23. Dong X, Erkey C, Dai HJ, Li HC, Cochran HD, Lin JS. Phase behavior and micelle size of an aqueous microdispersion in supercritical CO_2 with a novel surfactant. *Ind Eng Chem Res*. 2002;41:1038-1042.
24. Fremgen DE, Smotkin ES, Gerald RE, Klingler RJ, Rathke JW. Microemulsions of water in supercritical carbon dioxide: an in situ NMR investigation of micelle formation and structure. *J Supercrit Fluids*. 2001;19:287-298.
25. Jacobson GB, Lee CT, Johnston KP, Tumas W. Enhanced catalyst reactivity and separations using water/carbon dioxide emulsion. *J Am Chem Soc*. 1999;121:11902-11903.
26. Jacobson GB, Lee CT, Johnston KP. Organic synthesis in water/carbon dioxide microemulsions. *J Org Chem*. 1999;64:1201-1206.
27. Jacobson GB, Lee CT, daRocha RP, Johnston KP. Organic synthesis in water/carbon dioxide emulsions. *J Org Chem*. 1999;64:1207-1210.
28. Ohde H, Wai CM, Kim H, Kim J, Ohde M. Hydrogenation of olefins in supercritical CO_2 catalyzed by palladium nanoparticles in a water-in-CO_2 microemulsion. *J Am Chem Soc*. 2002;124:4540-4541.
29. Ohde M, Ohde H, Wai CM. Catalytic hydrogenation of arenes with rhodium nanoparticles in a water-in-supercritical CO_2 microemulsion. *Chem Commun*. 2002;20:2388-2389.
30. Bonilla RJ, James BR, Jessop PG. Colloid-catalyzed arene hydrogenation in aqueous/supercritical fluid biphasic media. *Chem Commun*. 2000;11:941-942.
31. McCarthy M, Stemmer H, Leitner W. Catalysis in inverted supercritical CO_2/aqueous biphasic media. *Green Chem*. 2002;4:501-504.
32. Holmes JD, Steytler DC, Rees GD, Robinson BH. Bioconversions in a water-in-CO_2 microemulsion. *Langmuir*. 1998;14:6371-6376.
33. Dong X, C Erkey C. Hydroformylation of olefins in water-in-carbon dioxide microemulsions. *ACS Symposium Series*. 2003;860:430-443.
34. Timko MT, Diffendal JM, Tester JW. Ultrasonic emulsification of liquid, near-critical carbon dioxide-water biphasic mixtures for acceleration of a hydrolysis reaction. *J Phys Chem A*. 2003;107:5503-5507.
35. Kumar A, Gogate PR, Pandit AB, Delmas H, Wilhelm AM. Gas-liquid mass transfer studies in sonochemical reactors. *Ind Eng Chem Res*. 2004;43:1812-1819.
36. Timko MT. *Acoustic Emulsions Of Liquid, Near-Critical Carbon Dioxide and Water: Application to Synthetic Chemistry Through Reaction Engineering*. Ph.D. Thesis, Dept. of Chemical Engineering, M.I.T., Cambridge, MA; 2004.
37. Mason TJ. *Practical Sonochemistry: User's Guide to Applications in Chemistry and Chemical Engineering*. New York: Ellis Horwood; 1991.
38. Nedhuzhii SA. Nature of the disturbances giving rise to formation of the disperse phase of an emulsion in an acoustic field. *Sov Phys Acoust*. 1965;10:390-397.
39. Canselier JP, Delmas H, Wilhelm AM, Abismaïl B. Ultrasound emulsification—an overview. *Ultrason Sono*. 2002;23:333-349.
40. Li MK, Fogler HS. Acoustic emulsification. Part I. The instability of the oil-water interface to form the initial droplets. *J Fluid Mech*. 1978;88:499-511.
41. Li MK, Fogler HS. Acoustic emulsification. Part II. The breakup of the large primary oil droplets in a water medium. *J Fluid Mech*. 1978;88:513-528.
42. Büttner D, Heydtmann H. The hydrolysis of 1–chloro 2–nitro ethane, chloro diphenyl methane and benzoyl chloride in dioxane–water mixtures at 1–1000 at. *Ber Bunsen*. 1969;73:640-646.
43. Al-Lohedan H, Bunton CA, Mhala MM. Micellar effects upon spontaneous hydrolyses and their relationship to mechanism. *J Am Chem Soc*. 1982;104:6654-6660.
44. Song BD, Jencks WP. Mechanism of solvolysis of substituted benzoyl halides. *J Am Chem Soc*. 1989;111:8470-8479.
45. Bunton CA, Gillitt ND, Mhala MM, Moffatt JR, Yatsimirsky AK. Micellar charge effects upon hydrolysis of substituted benzoyl chlorides. Their relationship to mechanism. *Langmuir*. 2000;16:8595-8603.
46. Bentley TW, Carter GE, Harris HC. S_N2 character of hydrolysis of benzoyl chloride. *J Chem Soc, Chem Commun*. 1984;6:387-389.
47. Bentley TW, Carter GE, Harris HC. Competing S_N2 and carbonyl addition pathways for solvolysis of benzoyl chloride in aqueous media. *J Chem Soc, Perkins Trans 2*. 1985;7:983-990.
48. Bentley TW, Harris HC. Solvolysis of *para*–substituted benzoyl chlorides in trifluoromethanol and in highly aqueous media. *J Chem Soc, Perkins Trans 2*. 1986;4:619-624.
49. Timko MT, Nicholson BF, Steinfeld JI, Smith KA, Tester JW. Partition coefficients of organic solutes between supercritical carbon dioxide and water: experimental measurements and empirical correlations. *J Chem Eng Data*. 2004;49:768-778.
50. Anderson DK, Hall JR, Babb AL. Mutual diffusion in nonideal binary liquid mixtures. *J Phys Chem*. 1958;62:404-408.
51. Gabler T, Paschke A, Schuurmann G. Diffusion coefficients of substituted benzenes at high dilution in water. *J. Chem. Eng. Data*. 1996;41:33-36.
52. Pradhan AA, Heideger WJ. On the measurement of liquid phase diffusivities for slightly soluble solids. *Can J Chem Eng*. 1971;49:10-13.
53. Reid RC, Prausnitz JM, Sherwood TK. *The Properties of Gases and Liquids*. 4th ed. New York: McGraw Hill; 1977.
54. King CV, Brodie SS. The rate of dissolution of benzoic acid in dilute aqueous alkali. *J Am Chem Soc*. 1937;59:1375-1379.
55. Linton WH, Sherwood TK. Mass transfer from solid shapes to water in streamline and turbulent flow. *Chem Eng Prog*. 1950;46:258-264.
56. Turitto VT. Mass transfer in annuli under conditions of laminar flow. *Chem Eng Sci*. 1975;30:503-509.
57. Vanadurongwan VC, Laguerie C, Couderc JP. Diffusivité moyenne de l'acide benzoique dans l'eau entre la dilution infinite et la saturation: influence de la temperature. *Can J Chem Eng*. 1976;54:460-463.
58. Ratcliff GA, Reid KJ. Mass transfer into spherical liquid films. Part I. Measurement of liquid diffusivities. *Trans Inst Chem Eng*. 1961;39:423-432.
59. Garner FH, Marchant PJM. Diffusivities of associated compounds in water. *Trans Inst Chem Eng*. 1961;39:397-408.
60. Bonoli L, Witherspoon PA. Diffusion of aromatic and cycloparaffin hydrocarbons in water from 2 to 60°. *J Phys Chem*. 1968;72:2532-2534.
61. Lewis JB. Some determinations of liquid-phase diffusion coefficients by means of an improved diaphragm cell. *J Appl Chem*. 1955;5:228-237.
62. Scholtz MT, Trass O. Mass transfer in laminar radial wall jet. *AIChE J*. 1963;9:548-554.
63. Bueno JL, Suarez JJ, Dizy J, Medina I. Infinite dilution diffusion coefficients: benzene derivatives as solutes in supercritical carbon dioxide. *J Chem Eng Data*. 1993;38:344-349.
64. Sassiat PR, Mourier P, Caude MH, Rosset RH. Measurement of diffusion coefficients in supercritical carbon dioxide and correlation with the equation of Wilke and Chang. *Anal Chem*. 1987;59:1164-1170.
65. Funazukuri T. Measurements of binary diffusion coefficients of 20 organic compounds in CO_2 at 313.2 K and 16.0 MPa. *J Chem Eng Jap*. 1996;29:191-192.
66. Suárez JJ, Bueno JJ, Medina I. Determination of binary diffusion coefficients of benzene and derivatives in supercritical carbon dioxide. *Chem Eng Sci*. 1993;48:2419-2427.
67. Filho CA, Silva CM, Quadri MB, Macedo EA. Infinite dilution diffusion coefficients of linalool and benzene in supercritical carbon dioxide. *J Chem Eng Data*. 2002;47:1351-1354.
68. Yang XN, Coelho LAF, Matthews MA. Near-critical behavior of mutual diffusion coefficients for five solutes in supercritical carbon dioxide. *Ind Eng Chem Res*. 2000;39:3059-3068.
69. Catchpole OJ, King MB. Measurement and correlation of binary diffusion coefficients in near critical fluids. *Ind Eng Chem Res*. 1994;33:1828-1837.
70. Brudi K, Dahmen N, Schmieder H. Partition coefficients of organic substances in two-phase mixtures of water and carbon dioxide at pressures of 8 to 30 MPa and temperatures of 313 to 333 K. *J Supercrit Fluids*. 1996;9:146-151.
71. Wagner K, Brudi K, Dahmen N, Schmieder H. Partition coefficients of organic substances in two-phase mixtures of water and carbon dioxide at pressures of 8 to 30 MPa and temperatures of 313 to 333 K. Part II. *J Supercrit Fluids*. 1999;15:109-116.
72. Sherwood TK, Pigford RL, Wilke CR. *Mass Transfer*. New York: McGraw–Hill; 1975.
73. Froment GF, Bischoff KB. *Chemical Reactor Analysis and Design*. New York: Wiley; 1979.

74. Danckwerts PV. *Gas–Liquid Reactions*. New York: McGraw–Hill; 1970.
75. Kuijpers MWA, van Eck D, Kemmere MF, Keurentjes JTF. Cavitation-induced reactions in high-pressure carbon dioxide. *Science*. 2002; 298:1969-1971.
76. Mason TJ. Large scale sonochemical processing: aspiration and actuality. *Ultrason Sono*. 2000;7:145-149.
77. Seymour JD, Wallace HC, Gupta RB. Sonochemical reactions at 640 kHz using an efficient reactor. Oxidation of potassium iodide. *Ultrason Sono*. 1997;4:289-293.
78. Henglein A, Gutiérrez M. Sonochemistry and sonoluminescence: effect of external pressure. *J Phys Chem*. 1993;97:158-162.
79. Wayment DG, Casadonte DJ. Design and calibration of a single–transducer variable-frequency sonication system. *Ultrason Sono*. 2002;9:189-195.
80. Hart EJ, Henglein A. Free radical and free atom reactions in the sonolysis of aqueous iodide and formate solutions. *J Phys Chem*. 1985;89:4342-4347.
81. Acrivos A, Taylor TD. Heat and mass transfer from single spheres in stokes flow. *Phys Fluids*. 1962;5:387-394.
82. Batchelor GK. Sedimentation in a dilute dispersion of spheres. *J Fluid Mech*. 1972;52:245-268.
83. Tai CY, You G, Chen S. Kinetics study on supercritical fluid extraction of zinc(II) ion from aqueous solutions. *J Supercrit Fluids*. 2000; 18:201-212.
84. Lewis JB. The mechanism of mass transfer of solutes across liquid-liquid interfaces. Part 2. The transfer of organic solutes between solvent and aqueous phases. *Chem Eng Sci*. 1954;3:260-278.
85. McManamey WJ. Molecular diffusion and liquid-liquid mass transfer in stirred transfer cells. *Chem Eng Sci*. 1961;15:251-254.
86. McManamey WJ, Davies JT, Woollen JM, Coe JR. The influence of molecular diffusion on mass transport between turbulent liquids. *Chem Eng Sci*. 1973;28:1061-1069.
87. Gogate PR, Pandit AB. Sonochemical reactors: scale-up aspects. *Ultrason Sono*. 2004;11:105-117.
88. Destaillats H, Lesko TM, Knowlton M, Wallace H, Hoffman MR. Scale-up of sonochemical reactors for water treatment. *Ind Eng Chem Res*. 2001;40:3855-3860.
89. Gogate PR, Sivakumar M, Pandit AB. Destruction of rhodamine B using novel sonochemical reactor with capacity of 7.5 L. *Sep Pur Tech*. 2004;34:13-24.
90. Bevington PR, Robinson DK. *Data Reduction and Error Analysis for the Physical Sciences*. 2nd ed. New York: McGraw–Hill, Inc.; 1992: 43.

Appendix A

The emulsion model described by Eq. 9 assumes that the concentration of reactant in the water droplets is uniform and always equals that in the bulk carbon dioxide phase divided by K_{CW}. This assumption is valid for $Da_W < 1$, as it was in our experiments. For $1 < Da_W < 10$, the concentration is no longer uniform. To extend our analysis to $1 < Da_W < 10$, the concentration profile in the droplets must be determined. The final expression for the volume averaged concentration is given by the following expression:

$$\frac{\langle [A]_{W,drop}\rangle_{volume}}{[A]_C/K_{CW}} = \frac{3}{Da_W \sinh(\sqrt{Da_W})} \times \{\sqrt{Da_W}\cosh(\sqrt{Da_W}) - \sinh(\sqrt{Da_W})\} \quad \text{(A1)}$$

Equation 9a can easily be modified by using this expression for $[A]_{W,drop}$. The error introduced by assuming a uniform profile is less than 20% provided that $Da_W < 3$ and less than 10% for $Da_W < 1$.

Appendix B

We used two different methods to estimate the effect of the uncertainties of physical parameters on predictions of k^*_{sonic}: (1) calculation of the range of k^*_{sonic} assuming that there was no cancellation of errors among the various parameters, and (2) propagation of the errors in physical parameters to estimate the standard deviation of k^*_{sonic}. We will demonstrate the difference between the two techniques using τ_{WM} as the test function:

$$\tau_{WM} = \frac{K_{CW}}{k_{rxn}}\frac{\underline{V}_C}{\underline{V}_W} \quad \text{(B1)}$$

For Method 1, we calculate the maximum τ_{WM} by inserting the highest values of k_{rxn} and $\underline{V}_W$ and the lowest values of K_{CW} and $\underline{V}_C$. For calculating the minimum of τ_{WM}, the method is reversed.

For Method 2, we use the standard formula for propagation of errors[90]:

$$\sigma^2_{k_{well\text{-}mixed}} \approx \sigma^2_{K_{CW}}\left(\frac{\partial k_{well\text{-}mixed}}{\partial K_{CW}}\right)^2 + \sigma^2_{k_{rxn}}\left(\frac{\partial k_{well\text{-}mixed}}{\partial k_{rxn}}\right)^2 + \cdots \quad \text{(B2)}$$

where we have implicitly assumed that cross correlation terms (i.e., $\sigma_{K_{CW}/k_{r\times N}}$, etc.) are negligibly small, which is almost certainly true. The standard deviation estimated from Method 2 is considerably smaller than the range estimated using Method 1, as it should be.

Manuscript received Mar. 14, 2005, and revision received Aug. 17, 2005.